3-12-2019

C–H/π and C–H–O Interactions in Concert: A Study of the Anisole–Methane Complex using Resonant Ionization and Velocity Mapped Ion Imaging

James Makuvaza

Damian Kokkin

John Loman

Scott A. Reid

Journal of Physical Chemistry : A, Vol. 123, No. 13 (March 12, 2019): 2874-2880. DOI.

C–H/π and C–H–O Interactions in Concert: A Study of the Anisole–Methane Complex using Resonant Ionization and Velocity Mapped Ion Imaging

James T. Makuvaza
Department of Chemistry, Marquette University, Milwaukee, Wisconsin
Damian L. Kokkin
Department of Chemistry, Marquette University, Milwaukee, Wisconsin
John L. Loman
Department of Chemistry, Marquette University, Milwaukee, Wisconsin
Scott A. Reid
Department of Chemistry, Marquette University, Milwaukee, Wisconsin

Abstract

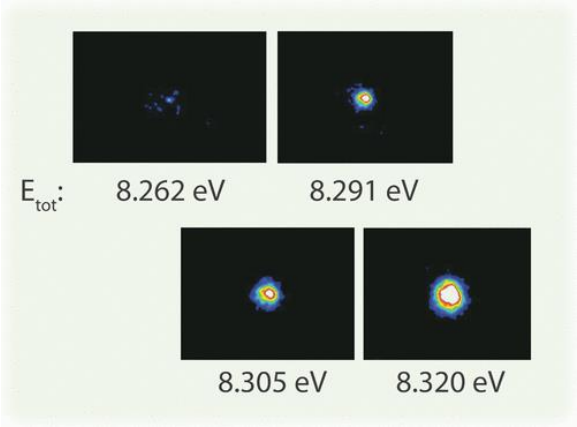

Noncovalent forces such as hydrogen bonding, halogen bonding, π–π stacking, and C–H/π and C–H/O interactions hold the key to such chemical processes as protein folding, molecular self-assembly, and drug–substrate interactions. Invaluable insight into the nature and strength of these forces continues to come from the study of isolated molecular clusters. In this work, we report on a study of the isolated anisole–methane complex, where both C–H/π and C–H/O interactions are possible, using a combination of theory and experiments that include mass-selected two-color resonant two-photon ionization spectroscopy, two-color appearance potential (2CAP) measurements, and velocity mapped ion imaging (VMI). Using 2CAP and VMI, we derive the binding energies of the complex in ground, excited, and cation radical states. The experimental values from the two methods are in excellent agreement, and they are compared with selected theoretical values calculated using density functional theory and ab initio methods. The optimized ground-state cluster geometry, which is consistent with the experimental observations, shows methane sitting above the ring, interacting with anisole via both C–H/π and C–H/O interactions, and this dual mode of interaction is reflected in a larger ground-state binding energy as compared with the prototypical benzene–methane system.

SPECIAL ISSUE

Published as part of *The Journal of Physical Chemistry* virtual special issue “Hanna Reisler Festschrift”.

Introduction

The characterization of isolated molecular clusters provides important insights into the nature and strength of intermolecular forces and noncovalent interactions,(1−5) which, in turn, impact a variety of fields, including protein folding,(6) supramolecular chemistry and molecular self-assembly,(7,8) crystal engineering,(9−11) and drug–substrate interactions.(12−14) Moreover, the study of intermolecular binding interactions and energetics in isolated clusters affords insight into the complex reality of solute–solvent interactions in condensed phases.(15,16) A variety of distinct noncovalent interactions are important, including hydrogen bonding,(17) halogen bonding and other σ-hole-type interactions,(18−20) π–π interactions,(3) C–H−π interactions,(10,21−28) and C–H–O interactions,(29,30) which can act in concert or in competition.

Many prior studies of weakly bound clusters have utilized a reference chromophore, often consisting of an aromatic moiety that can be spectroscopically detected via fluorescence or resonant ionization methods, bound to different species (e.g., rare gas, diatomic, or small polyatomic molecules) to probe the structure and strength of the interaction mechanism.(2,16,30−36) Isolated clusters can be readily prepared experimentally through use of jet-cooled supersonic expansions (molecular beams),(5,16,37−39) with electronic or infrared spectroscopy used to classify spectral changes of the chromophore upon cluster formation. The advent of velocity mapped ion imaging (VMI) has provided another tool for investigating the binding energies of clusters,(40−44) which the

Reisler group has exploited to measure the binding energies of a variety of model hydrogen-bonded complexes.(45−51) In the present article, we utilize anisole as a chromophore and employ resonant 2-photon ionization (R2PI) and VMI methods to probe the anisole–methane complex. Given that anisole possesses two sites that can act as proton acceptors, the electron lone pair on oxygen and its aromatic electron system, both C–H−π and C–H–O interactions may be expected. While relatively weak in comparison with hydrogen bonding, these are nonetheless important types of noncovalent interactions.(10,21,22,29,30)

Anisole is a prototypical aromatic chromophore,(52) readily detected via R2PI methods, and relevant for studying different intermolecular interactions, as evident by the variety of reported studies on the formation and characterization of molecular complexes of anisole with simple systems including CO_2,(33) NH_3,(53) H_2O,(31) and Ar.(54) In addition, the anisole dimer has been extensively studied.(32,35,55) With two main primary sites available as proton acceptors, it is noteworthy that the anisole–H_2O 1:1 complex exhibits a hydrogen bond with the oxygen lone pair, while the anisole–NH_3 1:1 complex is of a π-type. Motivated by these studies, we sought to consider the anisole–CH_4 1:1 complex, specifically as to how the geometry and C–H−π binding characteristics would be influenced by the methoxy substituent, in comparison to prior theoretical and experimental studies of aliphatic C–H/ π-type clusters of methane with various aromatics.(56−59)

Thus, in this work we present a combined experimental and theoretical investigation of the anisole–methane van der Waals complex. Experimentally, the spectroscopy and binding energies of the complex were determined using R2PI and VMI methods. First, the electronic spectrum of the complex was obtained using two-color R2PI (2CR2PI) spectroscopy with an ionizing photon of fixed wavelength (266 nm). Ionization potentials of the anisole monomer and anisole–methane complex were determined using ion yield spectra measured with 2CR2PI spectroscopy, using a tunable ionizing photon. Then, two-color appearance potential (2CAP) measurements were conducted on the isolated anisole–methane cluster to determine the binding energy in the ground (S_0) state, from which upper limits on binding energies in the first excited (S_1) and cation radical (D_0) states were obtained using a thermochemical cycle analysis. As a further check, we determined the binding energy in the D_0 state using VMI, which following application of the thermochemical cycle gave consistent values for the binding energy in all three component states. The experimental results were compared with theoretical predictions based on dispersion-corrected density functional theory (DFT), as well as ab initio methods.

Experimental and Theoretical Methods

We conducted several types of experiments for this work. R2PI and associated studies were performed in a 1 m linear time-of-flight (TOF) mass spectrometer, which has previously been described in detail.(2) In 2CR2PI experiments, the first photon, resonant with the S_0–S_1 transition, came from the frequency-doubled output of a Nd:YAG pumped dye laser (Lambda-Physik Scanmate 2E pumped by the third harmonic of a Quantel Q-Smart 850 Nd:YAG laser). The second ionizing photon came from either the 266 nm output of a second Nd:YAG system (Continuum Minilite) or the tunable frequency-doubled output of a second Nd:YAG pumped dye laser (Sirah Cobra-Stretch pumped by the second harmonic of a Spectra-Physics INDI Nd:YAG laser). The excitation and ionization lasers were overlapped spatially and temporally and counter-propagated through the TOF spectrometer. Temporal control of the experiment was achieved by use of an eight-channel digital pulse/delay generator (Berkeley Nucleonics 565).

Initially, electronic spectra of anisole and the anisole–methane complex were obtained using 2CR2PI spectroscopy with 266 nm ionization, monitoring the monomer or complex mass, respectively. These spectra are shown in the lower panels of Figure 1. Ionization yield spectra (Figure 1, upper panels) were then obtained using a tunable ionization laser, where the pump laser wavelength (λ_1) was set on resonance of the monomer or complex, and the ionizing wavelength (λ_2) was scanned through the ionization threshold, while monitoring the

appropriate mass channel. Note that, for the electronic spectra in Figure 1, we use traditional spectroscopic units of inverse centimeters, whereas the ion yield spectra are given in electronvolts, with the energy representing the sum of the two photon energies. The counterpropagating lasers were loosely focused into the extraction region via 1.0 m (pump) or 2.0 m (probe) plano-convex focusing lenses and intersected perpendicularly with the supersonic molecular beam. In two-color experiments, the energy of the pump laser was attenuated using a polarizer such that no one-color signal from the pump laser was observed. The molecular beam was formed by passing a premix of 10% methane in Ar carrier gas, at backing pressures ranging between 40 and 80 psi, through a bubbler containing liquid anisole (Sigma-Aldrich, 99% purity) held in a refrigerated bath maintained at −5 °C. This mixture was expanded into the source chamber via the 0.8 mm diameter orifice of a pulsed nozzle (General Valve series 9), passing into the extraction region through a 1.5 mm diameter conical nickel skimmer (Beam Dynamics).

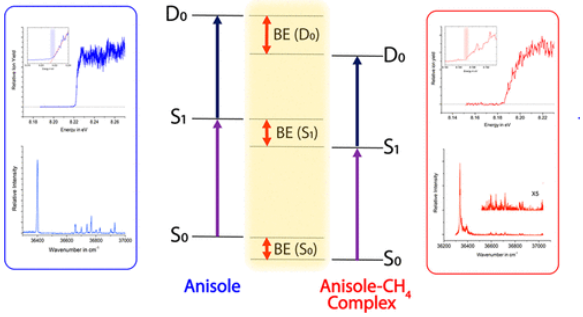

Figure 1. A snapshot of spectroscopic data obtained for jet-cooled anisole and the anisole–methane complex, together with an energy ladder diagram. For each species, electronic spectra (S_0–S_1) were obtained in 2CR2PI experiments as described in the text (lower figure in each panel). Ion yield spectra were then obtained in 2CR2PI measurements using a tunable second photon, to determine the ionization thresholds (upper figure in each panel). As shown, ion yield spectra for both species exhibited sharp thresholds, indicative of modest geometry changes upon ionization.

One complication observed was the presence of an anisole hot band, likely the $6B_1^1$ transition, which overlapped the origin band of the anisole–methane complex. While this, of course, was not a hindrance for spectroscopic experiments where the cluster ion was detected, it proved a nuisance in determination of the complex dissociation energy using the 2CAP and VMI methods, where the *monomer* ion was detected. There, we found it necessary to operate at higher backing pressures and tweak the nozzle-laser delay conditions to minimize the intensity of this feature.

Velocity-mapped ion imaging experiments were performed in a separate, newly constructed spectrometer that utilized the same molecular beam source. The source chamber was differentially pumped by a 6 in. diffusion pump (VHS-6), and the molecular beam entered the ionization region by passing through a 1.5 mm diameter conical nickel skimmer (Beam Dynamics). The ion optic assembly, contained in a large cylindrical chamber pumped by an 8 in. diameter turbomolecular pump, consisted of a set of eleven 100 mm diameter, 1.5 mm thick polished steel electrodes. Electrodes 1–5 were separated by ceramic spacers 6.35 mm in diameter and 20 mm in length, while the remaining electrodes were separated by spacers of the same diameter and 25 mm in length. This electrode stack was mounted via another set of 25 mm long spacers onto a large (200 mm diameter, 2.0 mm thick) mounting plate. The central holes in these plates were 5 mm for the mounting plate, and, respectively, 5 mm for the first electrode, 25 mm for the second and third electrodes, and 40 mm for the remaining electrodes. Prior to mounting, the electrodes were coated with a thin layer of colloidal graphite.

The laser(s) crossed the molecular beam between the first (repeller) and second (extractor) electrode, at a point 150 mm downstream of the skimmer orifice. In the experiments reported here, the repeller and extractor electrodes were biased at 2000 V and ∼1380 V, respectively, with the voltages tuned precisely (in ±1 V

increments, using Stanford Research Systems PS325 high-voltage power supplies) to obtain velocity mapping conditions. The remaining electrodes were grounded. To aid initially in finding the appropriate velocity mapping conditions, ion trajectories were simulated using SIMION 8.1 software.

The imaging detector was contained in a separate chamber pumped by a 6 in. turbomolecular pump, which could be isolated from the main flight tube using a gate valve. The base pressure in the detection region was typically 1×10^{-8} Torr. The detector was mounted coaxially with the molecular beam at a point 1.3 m downstream of the skimmer and consisted of a VID275 camera system (Photek), which incorporated a dual 75 mm chevron microchannel plate (MCP) stack interfaced with an image intensifier and IDS UI3060 camera. The MCP input was grounded, and the front and rear MCP voltages were typically set at 850 and 1700 V, respectively. The screen voltage was typically set at 5000 V; all voltages were supplied via a tracking, triple output digital high-voltage power supply (Photek). To collect images only on the mass feature of interest, the rear MCP voltage was lowered by 500 V, and a variable gate pulse of +500 V amplitude was alternating current (AC) coupled to the rear MCP using a separate gate unit.

Ion images were typically acquired over thousands of laser shots (18 000 for a typical 30 min integration), with the signal attenuated to observe only a few ions each laser shot to avoid image blurring from space charge effects. The resultant images were background-subtracted using images obtained with λ_2 set below the fragmentation threshold, and the inverse Abel transform of the images was calculated using the pBASEX algorithm in a LABVIEW coded program.(60) To calibrate the images, we measured the binding energy of the anisole–Ar 1:1 complex, which has been precisely determined (with a precision of <1%) using mass-analyzed threshold ionization.(54) The derived instrumental magnification factor was in good agreement with that estimated from SIMION simulations.

To support our experimental findings, electronic structure calculations were performed using the Gaussian 09 software package.(61) In a study of the benzene dimer, we previously found that accurate ground- and excited-state energies could be obtained using a simple PBE0 density functional(62−64) augmented with the D3 version of Grimme's dispersion term.(65) More recent studies of fluorene-based complexes revealed that the CAM-B3LYP-D3 method well-reproduced experimental binding energies across neutral, excited, and cation radical states. Thus, calculations of the ground-state binding energy were initially performed using PBE0-D3 and CAM-B3LYP-D3 methods with QZVPPD and 6-311++g(3df,3pd) basis sets.(66,67) The binding energies were corrected for zero-point energy and basis set superposition error using the counterpoise method—the latter was negligibly small with this quality of basis set. Geometry optimizations employed an ultrafine Lebedev's grid with 99 radial shells per atom and 590 angular points in each shell; tight cutoffs were employed.

Considering theoretical studies of the cation radical state, earlier studies of π-stacked complexes found that a calibrated(68−70) B1LYP functional with 40% of Hartree–Fock exchange (B1LYP-40) well-reproduced properties of the cation radical state. However, this method performed poorly in the present case, and we thus turned to the MP2 method, which has previously been benchmarked (with aug-cc-pVXZ basis sets, X = D or T) for quantitative evaluation of C–H/π interaction energies.(24) Additionally, other dispersion-corrected DFT methods were used to examine the cation radical state.

Results and Discussion

Figure 1 shows an overview of some of the spectroscopic information collected on anisole and the anisole–methane complex, presented with energy ladders for the monomer and complex in the S_0, S_1, and D_0 (cation radical) states. The electronic spectra of anisole, which is similar to that previously reported,(71,72) and the complex were obtained using 2CR2PI spectroscopy as described above, and they are shown in the lower panels in Figure 1. The spectrum of the complex is origin-dominated, indicative of a small geometry change upon

electronic excitation, and the origin is red-shifted by −64 cm^{-1} from that of anisole (see also Figure S1 in the Supporting Information). This shift is significantly larger than that observed for the benzene–methane (−41 cm^{-1}) or toluene–methane (−43 cm^{-1}) complexes.(59,73) The S_1 vibrational frequencies derived from these spectra, given in Table S1 in the Supporting Information, show very little shift in the low-frequency aromatic ring vibrations upon complexation.

With the electronic spectrum of the complex determined, we performed 2CR2PI measurements of the monomer and complex with a tunable ionizing photon to determine the respective ionization thresholds. Both species exhibited sharp ionization onsets (see the upper panels of Figure 1) from which the following IPs were obtained: anisole, 8.222(5) eV; the anisole–methane complex, 8.186(5) eV—one standard deviation is given in parentheses. As the *difference* in these values will be emphasized here, our measurements were uncorrected for shifts due to electrostatic fields in the mass spectrometer. Note that our measured value for anisole is slightly lower than prior determinations (8.232 eV).(74,75)

Following this initial spectroscopic characterization of the complex, we then performed 2CAP measurements.(39,55,76) In this method, which provides an upper limit to the binding energy in the S_0 state and is illustrated in Figure 2A, the excitation wavelength (λ_1) is fixed on resonance of the complex, and the ionizing photon wavelength (λ_2) is scanned above the cluster IP while monitoring the yield of the *monomer* (anisole) cation. The energetic onset marking the appearance of the anisole cation represents the sum of the adiabatic monomer ionization energy (AIE) and ground-state complex binding energy (Figure 2A). In Figure 2B is the measured 2CAP spectrum, in which the *x*-axis scale was set by subtracting the monomer IP from the two-photon energy, yielding a ground-state binding energy (given in eV). Two clear onsets are observed in the 2CAP spectrum. The onset at lower energy represents ionization from a hot-band of the monomer. This could be reduced but not entirely eliminated by varying the expansion conditions. The higher onset represents the true appearance potential of the monomer from cracking of the anisole–methane complex, which was determined via a linear extrapolation as shown. This approach yielded a ground (S_0) state binding energy upper limit of 0.060(2) eV, or, in the more traditional unit for complex binding energies, 5.8(2) kJ/mol. Application of the thermochemical cycle shown in Figure 1 then returned binding energy upper limits in S_1 and D_0 of, respectively, 6.6(2) and 9.2(2) kJ/mol. These are provided in Table1.

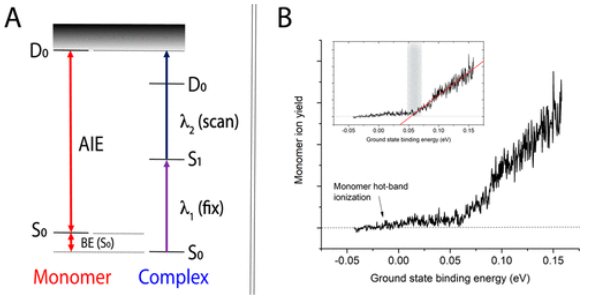

Figure 2. (A) Illustration of the 2CAP method. The appearance energy of the monomer fragment equals the sum of monomer AIE and ground-state complex binding energy. (B) 2CAP spectrum of the anisole–methane complex, with the energy axis scaled to show the ground-state binding energy. The lower energy threshold represents excitation of a monomer hot-band transition, while the higher energy threshold is associated with the complex. Linear extrapolation of a fit of the rising edge of this feature (inset) returns the ground-state binding energy of the complex.

Table 1. Comparison of Experimental and Computed Binding Energies for the Anisole–Methane Complex[a]

	binding energy (kJ/mol)		
method	S_0	S_1	D_0
experiment (2CAP)	**5.8(2)**	**6.6(2)**	**9.2(2)**
experiment (VMI)	**5.79(13)**	**6.56(13)**	**9.22(13)**
CAM-B3LYP-D3/def2-QZVPPD	**5.2**		

CAM-B3LYP-D3/6-311++g(3df,3pd)	**5.3**		**9.1**
PBE0-D3/def2-QZVPPD	**6.1**		
PBE0-D3/6-311++g(3df,3pd)	**6.6**		**10.5**
B3LYP-D3/6-311++g(3df,3pd)	**5.5**		**9.4**
M06-2*X*/6-311++g(3df,3pd)	**5.4**		**9.5**
MP2/6-311++g(3df,3pd)	**5.8**		
MP2/aug-cc-pVTZ[b]	**6.0**		**6.6**

[a]All calculated binding energies were corrected for zero-point energy and basis set superposition error using the counterpoise method. For the cation radical state, spin-unrestricted wavefunctions were employed. Experimental values list one standard deviation in parentheses.
[b]Single-point calculation based on structure optimized (and zero-point energy corrections) at MP2/aug-cc-pVDZ level.

An alternative strategy to determine the cluster binding energy in the D_0 state is VMI.(40−44) Here, the complex is selectively excited via two-color excitation to energies above the dissociation energy in D_0, and the kinetic energy (KE) release in the monomeric (anisole) cationic fragment is measured. Under the assumption that the maximum observed kinetic energy release corresponds to the production of two fragments with zero internal energies, that is

$$KE_{\max} = E^{\dagger} = E_{\text{photon}} - \text{BE}(\text{D}_0) \quad (1)$$

the binding energy (BE) in D_0 is determined. Application of the thermochemical cycle shown in Figure 1 then returns the S_0 and S_1 binding energies. In practice, the VMI method also sets an upper limit to the binding energy, as signal/noise limitations may lead to an observed KE_{max} smaller than the true value. Moreover, on the one hand, the internal energy distribution in the counter fragment is not known. On the other hand, it is important to limit the number of ions formed per shot, particularly with the long path length employed here, as space charge effects can blur the image, potentially leading to an overestimate of KE_{max}.

The upper panel of Figure 3 displays VMI images of the anisole cation obtained following ionization of the anisole–methane complex at the total energies shown, while the lower panel displays the kinetic energy distributions obtained from transformation of the images obtained at three wavelengths above threshold. As the total energy increases above threshold, KE_{max} (eq 1) also clearly increases, as expected. Upon the basis of the observed KE_{max} and the available total energy, a cluster binding energy in D_0 was determined at each data point and averaged over measurements obtained at different ionizing photon wavelengths. The corresponding binding energy values in S_0 and S_1 were obtained using the thermochemical cycle shown in Figure 1, and all binding energies are recorded with one standard deviation in Table1. It is immediately noted that the VMI results are in excellent agreement with the values derived from 2CAP measurements.

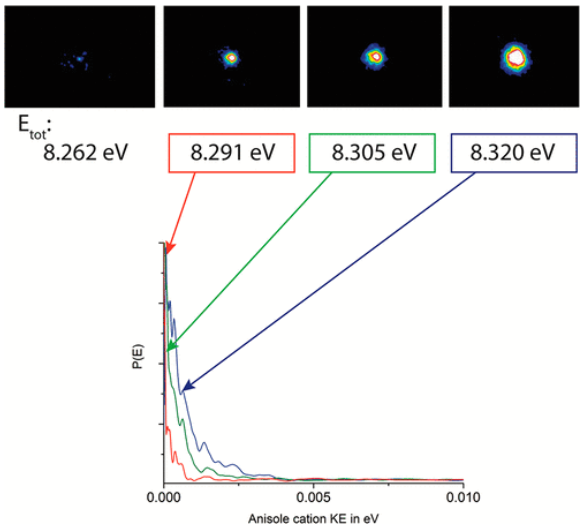

Figure 3. (upper) Anisole monomer ion images obtained following fragmentation of the ionized anisole–methane complex at four different total energies, corresponding to one energy below (left) and three energies above (lower) the complex fragmentation threshold. *P*(*E*) distributions derived following transformation of the images obtained above threshold, as described in the text. The *x*-axis labels the anisole cation kinetic energy in electronvolts. The maximum kinetic energy values derived from these plots were used to calculate the complex binding energy in the D_0 state, as described in the text.

Shown also in Table1 are a selection of calculated binding energies obtained at different levels of theory. Unless otherwise noted, these were obtained following complete geometry optimization of the complex and monomers, and they are corrected for zero-point energy and basis set superposition error (BSSE) using the counterpoise method. Note that the optimized cluster structure was similar among the various methods. Focusing first on the ground (S_0) state, the calculated binding energies are largely in good agreement with experiment, ranging from 5.2 to 6.6 kJ/mol. Figure 4 shows two views of the optimized structure of the complex at the PBE0-D3/def2-QZVPPD level of theory, where the methane is sitting above the plane of the ring, with one C–H group interacting with the O atom and a second interacting with the π-system of the aromatic ring (Figure 4A). This is more clearly seen in the alternate view shown in Figure 4B.

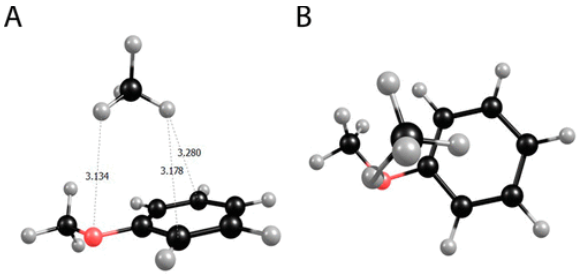

Figure 4. (A) Optimized structure of the ground (S_0) state of the anisole–methane complex at the PBE0-D3/def2-QZVPPD level of theory. (B) Alternate view illustrating the presence of both C–H/O and C–H/π interactions in the complex.

With respect to the D_0 state, the structure of the cation radical was optimized at various levels of theory, and the binding energies derived (Table1) were corrected for zero-point energy and BSSE using the counterpoise correction. Here spin-unrestricted wave functions were employed, and it was assumed in defining the fragments that the ionized complex consisted of an anisole cation radical and neutral methane. The optimized structure at the UMP2/aug-cc-pVDZ level, shown in Figure S2 in the Supporting Information, is similar to that of the ground state, consistent with our expectation of a modest geometry change from S_0 to D_0 based upon the origin-dominated S_0–S_1 transition and relatively sharp ionization onset observed in the experimental data (Figure 1). The calculated binding energies using various DFT methods are largely in good agreement with experiment,

while the single-point UMP2/aug-cc-pVTZ energy calculated based upon the structure optimized at the UMP2/aug-cc-pVDZ level is ∼25% smaller than measured experimentally. In future studies, we plan a more comprehensive theoretical treatment of this complex, which will also examine the binding energy in S_1.

While there are very few direct binding energy measurements of aromatic–methane clusters,(39) it is instructive to compare our results with prior experimental and theoretical studies of the related methane–benzene system. Here, ab initio calculations suggest that the ground state adopts a C_{3v} structure, where the methane sits above the ring, with one methane C–H bond interacting via C–H/π interaction with the aromatic ring.(56) Experimental measurement of the ground-state (S_0) binding energy using mass-analyzed threshold ionization (MATI) spectroscopy gives values of 4.31–4.73 kJ/mol,(24) in good agreement with the estimated CCSD(T) theoretical value at the complete basis set limit.(56) While experimentally measured binding energies of model C–H/O systems involving methane are lacking, theoretical calculations at the MP2 level suggest a binding energy for the CH_4–H_2O complex of ∼1 kJ/mol.(77) Thus, in comparison with benzene–methane, the larger ground-state binding energy measured here for anisole–methane is consistent with the dual role of C–H/π and C–H/O interactions in stabilizing the complex.

Conclusions

We have reported an experimental and theoretical investigation of the anisole–methane complex, a prototypical system for examining C–H/π and C–H/O interactions acting in concert. Indeed, the optimized ground-state structure of the complex, which gives a binding energy in excellent agreement with experiment, shows that both types of interactions are operative. Using two-color appearance potential and velocity mapped ion imaging experiments, we have derived binding energies for the complex in ground (S_0), excited (S_1), and cation radical (D_0) states. These are largely in good agreement with theoretical expectations.

Supporting Information

One table of vibrational frequencies for the anisole–methane complex and two additional figures. The Supporting Information is available free of charge on the ACS Publications website at DOI: 10.1021/acs.jpca.9b01020.
(PDF)
pdf
jp9b01020_si_001.pdf (175.99 kb)

References

1 Schneider, H. J. Non-Covalent Interactions. *J. Phys. Org. Chem.* **1997**, *10*, 253– 253, DOI: 10.1002/(SICI)1099-1395(199705)10:5<253::AID-POC1875>3.0.CO;2-R

2 Muzangwa, L.; Nyambo, S.; Uhler, B.; Reid, S. A. On Pi-Stacking, C-H/Pi, and Halogen Bonding Interactions in Halobenzene Clusters: Resonant Two-Photon Ionization Studies of Chlorobenzene. *J. Chem. Phys.* **2012**, *137*, 184307, DOI: 10.1063/1.4765102

3 Kim, K. S.; Tarakeshwar, P.; Lee, J. Y. Molecular Clusters of Pi-Systems: Theoretical Studies of Structures, Spectra, and Origin of Interaction Energies. *Chem. Rev.* **2000**, *100*, 4145– 4185, DOI: 10.1021/cr990051i

4 Gadre, S. R.; Yeole, S. D.; Sahu, N. Quantum Chemical Investigations on Molecular Clusters. *Chem. Rev.* **2014**, *114*, 12132– 12173, DOI: 10.1021/cr4006632

5 Buck, U. Structure and Dynamics of Size Selected Molecular Clusters. *Ber. Bunsen Phys. Chem.* **1992**, *96*, 1275– 1284, DOI: 10.1002/bbpc.19920960941

6 Zondlo, N. J. Non-Covalent Interactions. Fold Globally, Bond Locally. *Nat. Chem. Biol.* **2010**, *6*, 567– 568, DOI: 10.1038/nchembio.413

7 Rinaudo, M. Non-Covalent Interactions in Polysaccharide Systems. *Macromol. Biosci.* **2006**, *6*, 590– 610, DOI: 10.1002/mabi.200600053

8 Tkatchenko, A.; Alfe, D.; Kim, K. S. First-Principles Modeling of Non-Covalent Interactions in Supramolecular Systems: The Role of Many-Body Effects. *J. Chem. Theory Comput.* **2012**, *8*, 4317– 4322, DOI: 10.1021/ct300711r

9 LeBlanc, L. M.; Weatherby, J. A.; Otero-de-la-Roza, A.; Johnson, E. R. Non-Covalent Interactions in Molecular Crystals: Exploring the Accuracy of the Exchange-Hole Dipole Moment Model with Local Orbitals. *J. Chem. Theory Comput.* **2018**, *14*, 5715– 5724, DOI: 10.1021/acs.jctc.8b00797

10 Nishio, M. Ch/Pi Hydrogen Bonds in Crystals. *CrystEngComm* **2004**, *6*, 130– 158, DOI: 10.1039/b313104a

11 Metrangolo, P.; Resnati, G.; Pilati, T.; Biella, S. Halogen Bonding in Crystal Engineering. *Struct. Bonding (Berlin)* **2008**, *126*, 105– 136, DOI: 10.1007/430_2007_060

12 Morelli, X.; Rigby, A. C. Acceleration of the Drug Discovery Process: A Combinatorial Approach Using Nmr Spectroscopy and Virtual Screening. *Curr. Comput.-Aided Drug Des.* **2007**, *3*, 33– 49, DOI: 10.2174/157340907780058718

13 Britschgi, M.; von Greyerz, S.; Burkhart, C.; Pichler, W. J. Molecular Aspects of Drug Recognition by Specific T Cells. *Curr. Drug Targets* **2003**, *4*, 1– 11, DOI: 10.2174/1389450033347082

14 Yoon, H. J.; Jang, W. D. Polymeric Supramolecular Systems for Drug Delivery. *J. Mater. Chem.* **2010**, *20*, 211– 222, DOI: 10.1039/B910948J

15 Bartell, L. S. Structure and Transformation: Large Molecular Clusters as Models of Condensed Matter. *Annu. Rev. Phys. Chem.* **1998**, *49*, 43– 72, DOI: 10.1146/annurev.physchem.49.1.43

16 Jortner, J.; Even, U.; Goldberg, A.; Schek, I.; Raz, T.; Levine, R. D. Energetics and Dynamics of Molecular Clusters. *Surf. Rev. Lett.* **1996**, *3*, 263– 280, DOI: 10.1142/S0218625X96000516

17 Castellano, R. K. Special Issue: Intramolecular Hydrogen Bonding. *Molecules* **2014**, *19*, 15783– 15785, DOI: 10.3390/molecules191015783

18 Politzer, P.; Murray, J. S. Halogen Bonding: An Interim Discussion. *ChemPhysChem* **2013**, *14*, 278– 294, DOI: 10.1002/cphc.201200799

19 Clark, T.; Hennemann, M.; Murray, J. S.; Politzer, P. Halogen Bonding: The Sigma-Hole. *J. Mol. Model.* **2007**, *13*, 291– 296, DOI: 10.1007/s00894-006-0130-2

20 Politzer, P.; Murray, J. S.; Clark, T.; Resnati, G. The Sigma-Hole Revisited. *Phys. Chem. Chem. Phys.* **2017**, *19*, 32166– 32178, DOI: 10.1039/C7CP06793C

21 Re, S.; Nagase, S. How Is the Ch/Pi Interaction Important for Molecular Recognition?. *Chem. Commun.* **2004**, 658– 659, DOI: 10.1039/B316280J

22 Nishio, M.; Umezawa, Y.; Honda, K.; Tsuboyama, S.; Suezawa, H. Ch/Pi Hydrogen Bonds in Organic and Organometallic Chemistry. *CrystEngComm* **2009**, *11*, 1757– 1788, DOI: 10.1039/b902318f

23 Morita, S.; Fujii, A.; Mikami, N.; Tsuzuki, S. Origin of the Attraction in Aliphatic C-H/Pi Interactions: Infrared Spectroscopic and Theoretical Characterization of Gas-Phase Clusters of Aromatics with Methane. *J. Phys. Chem. A* **2006**, *110*, 10583– 10590, DOI: 10.1021/jp064297k

24 Shibasaki, K.; Fujii, A.; Mikami, N.; Tsuzuki, S. Magnitude of the Ch/Pi Interaction in the Gas Phase: Experimental and Theoretical Determination of the Accurate Interaction Energy in Benzene-Methane. *J. Phys. Chem. A* **2006**, *110*, 4397– 4404, DOI: 10.1021/jp0605909

25 Shibasaki, K.; Fujii, A.; Mikami, N.; Tsuzuki, S. Magnitude and Nature of Interactions in Benzene-X (X = Ethylene and Acetylene) in the Gas Phase: Significantly Different Ch/Pi Interaction of Acetylene as Compared with Those of Ethylene and Methane. *J. Phys. Chem. A* **2007**, *111*, 753– 758, DOI: 10.1021/jp065076h

26 Fujii, A.; Shibasaki, K.; Kazama, T.; Itaya, R.; Mikami, N.; Tsuzuki, S. Experimental and Theoretical Determination of the Accurate Interaction Energies in Benzene-Halomethane: The Unique Nature of the

Activated Ch/Pi Interaction of Haloalkanes. *Phys. Chem. Chem. Phys.* **2008**, *10*, 2836– 2843, DOI: 10.1039/b717053j

27 Tsuzuki, S.; Honda, K.; Fujii, A.; Uchimaru, T.; Mikami, M. Ch/Pi Interactions in Methane Clusters with Polycyclic Aromatic Hydrocarbons. *Phys. Chem. Chem. Phys.* **2008**, *10*, 2860– 2865, DOI: 10.1039/b718550b

28 Fujii, A.; Hayashi, H.; Park, J. W.; Kazama, T.; Mikami, N.; Tsuzuki, S. Experimental and Theoretical Determination of the Accurate Ch/Pi Interaction Energies in Benzene-Alkane Clusters: Correlation between Interaction Energy and Polarizability. *Phys. Chem. Chem. Phys.* **2011**, *13*, 14131– 14141, DOI: 10.1039/c1cp20203k

29 Tsuzuki, S.; Uchimaru, T.; Mikami, M. Magnitude of Ch/O Interactions between Carbohydrate and Water. *Theor. Chem. Acc.* **2012**, *131*, 131, DOI: 10.1007/s00214-012-1192-0

30 Scheiner, S.; Kar, T. Spectroscopic and Structural Signature of the Ch-O Hydrogen Bond. *J. Phys. Chem. A* **2008**, *112*, 11854– 11860, DOI: 10.1021/jp806984g

31 Reimann, B.; Buchhold, K.; Barth, H. D.; Brutschy, B.; Tarakeshwar, P.; Kim, K. S. Anisole-(H2o)(N) (N = 1–3) Complexes: An Experimental and Theoretical Investigation of the Modulation of Optimal Structures, Binding Energies, and Vibrational Spectra in Both the Ground and First Excited States. *J. Chem. Phys.* **2002**, *117*, 8805– 8822, DOI: 10.1063/1.1510443

32 Pietraperzia, G.; Pasquini, M.; Schiccheri, N.; Piani, G.; Becucci, M.; Castellucci, E.; Biczysko, M.; Bloino, J.; Barone, V. The Gas Phase Anisole Dimer: A Combined High-Resolution Spectroscopy and Computational Study of a Stacked Molecular System. *J. Phys. Chem. A* **2009**, *113*, 14343– 14351, DOI: 10.1021/jp903236z

33 Becucci, M.; Mazzoni, F.; Pietraperzia, G.; Rezac, J.; Natchigallova, D.; Hobza, P. Non-Covalent Interactions in Anisole-(Co2)(N) (N = 1, 2) Complexes. *Phys. Chem. Chem. Phys.* **2017**, *19*, 22749– 22758, DOI: 10.1039/C7CP03763E

34 Mazzoni, F.; Pasquini, M.; Pietraperzia, G.; Becucci, M. Binding Energy Determination in a Pi-Stacked Aromatic Cluster: The Anisole Dimer. *Phys. Chem. Chem. Phys.* **2013**, *15*, 11268– 11274, DOI: 10.1039/c3cp50191d

35 Schiccheri, N.; Pasquini, M.; Piani, G.; Pietraperzia, G.; Becucci, M.; Biczysko, M.; Bloino, J.; Barone, V. Integrated Experimental and Computational Spectroscopy Study on Pi-Stacking Interaction: The Anisole Dimer. *Phys. Chem. Chem. Phys.* **2010**, *12*, 13547– 13554, DOI: 10.1039/c002992k

36 Knochenmuss, R.; Sinha, R. K.; Leutwyler, S. Intermolecular Dissociation Energies of Dispersively Bound Complexes of Aromatics with Noble Gases and Nitrogen. *J. Chem. Phys.* **2018**, *148*, 134302, DOI: 10.1063/1.5019432

37 Stace, T. Chemical Physics - Cooling of Molecular Clusters. *Nature* **1987**, *327*, 186– 187, DOI: 10.1038/327186a0

38 Herschbach, D. Chemical Physics: Molecular Clouds, Clusters, and Corrals. *Rev. Mod. Phys.* **1999**, *71*, S411– S418, DOI: 10.1103/RevModPhys.71.S411

39 Frey, J. A.; Holzer, C.; Klopper, W.; Leutwyler, S. Experimental and Theoretical Determination of Dissociation Energies of Dispersion-Dominated Aromatic Molecular Complexes. *Chem. Rev.* **2016**, *116*, 5614– 5641, DOI: 10.1021/acs.chemrev.5b00652

40 Eppink, A. T. J. B.; Parker, D. H. Velocity Map Imaging of Ions and Electrons Using Electrostatic Lenses: Application in Photoelectron and Photofragment Ion Imaging of Molecular Oxygen. *Rev. Sci. Instrum.* **1997**, *68*, 3477– 3484, DOI: 10.1063/1.1148310

41 Bellm, S. M.; Moulds, R. J.; van Leeuwen, M. P.; Lawrance, W. D. A Velocity Map Ion Imaging Study of Difluorobenzene-Water Complexes: Binding Energies and Recoil Distributions. *J. Chem. Phys.* **2008**, *128*, 114314, DOI: 10.1063/1.2896081

42 Sampson, R. K.; Bellm, S. M.; Gascooke, J. R.; Lawrance, W. D. Velocity- and Mass-Resolved Rempi Spectroscopy of Van Der Waals Molecules. A Technique for Determining the Cluster Size Responsible for Spectral Features. *Chem. Phys. Lett.* **2003**, *372*, 307– 313, DOI: 10.1016/S0009-2614(03)00154-4

43 Bellm, S. M.; Gascooke, J. R.; Lawrance, W. D. The Dissociation Energy of Van Der Waals Complexes Determined by Velocity Map Imaging: Values for S-0 and S-1 P-Difluorobenzene-Ar and D-0 (P-Difluorobenzene-Ar). *Chem. Phys. Lett.* **2000**, *330*, 103– 109, DOI: 10.1016/S0009-2614(00)01063-0

44 Sampson, R. K.; Lawrance, W. D. The Dissociation Energy of the Benzene-Argon Van Der Waals Complex Determined by Velocity Map Imaging. *Aust. J. Chem.* **2003**, *56*, 275– 277, DOI: 10.1071/CH03050

45 Samanta, A. K.; Czako, G.; Wang, Y. M.; Mancini, J. S.; Bowman, J. M.; Reisler, H. Experimental and Theoretical Investigations of Energy Transfer and Hydrogen-Bond Breaking in Small Water and Hci Clusters. *Acc. Chem. Res.* **2014**, *47*, 2700– 2709, DOI: 10.1021/ar500213q

46 Reisler, H. Photofragment Spectroscopy and Predissociation Dynamics of Weakly Bound Molecules. *Annu. Rev. Phys. Chem.* **2009**, *60*, 39– 59, DOI: 10.1146/annurev.physchem.040808.090441

47 Samanta, A. K.; Wang, Y. M.; Mancini, J. S.; Bowman, J. M.; Reisler, H. Energetics and Predissociation Dynamics of Small Water, Hcl, and Mixed Hcl-Water Clusters. *Chem. Rev.* **2016**, *116*, 4913– 4936, DOI: 10.1021/acs.chemrev.5b00506

48 Mollner, A. K.; Casterline, B. E.; Ch'ng, L. C.; Reisler, H. Imaging the State-Specific Vibrational Predissociation of the Ammonia-Water Hydrogen-Bonded Dimer. *J. Phys. Chem. A* **2009**, *113*, 10174– 10183, DOI: 10.1021/jp904566w

49 Mollner, A. K.; Casterline, B. E.; Ch'ng, L. C.; Reisler, H. Imaging the State-Specific Vibrational Predissociation of the Ammonia-Water Hydrogen-Bonded Dimer (Vol 113a, Pg 10174, 2009). *J. Phys. Chem. A* **2010**, *114*, 1602– 1602, DOI: 10.1021/jp910008f

50 Parr, J. A.; Li, G.; Fedorov, I.; McCaffery, A. J.; Reisler, H. Imaging the State-Specific Vibrational Predissociation of the C2h2-Nh3 Hydrogen-Bonded Dimer. *J. Phys. Chem. A* **2007**, *111*, 7589– 7598, DOI: 10.1021/jp070838+

51 Li, G. S.; Parr, J.; Fedorov, I.; Reisler, H. Imaging Study of Vibrational Predissociation of the Hcl-Acetylene Dimer: Pair-Correlated Distributions. *Phys. Chem. Chem. Phys.* **2006**, *8*, 2915– 2924, DOI: 10.1039/B603107B

52 Bloino, J.; Biczysko, M.; Crescenzi, O.; Barone, V. Integrated Computational Approach to Vibrationally Resolved Electronic Spectra: Anisole as a Test Case. *J. Chem. Phys.* **2008**, *128*, 244105, DOI: 10.1063/1.2943140

53 Biczysko, M.; Piani, G.; Pasquini, M.; Schiccheri, N.; Pietraperzia, G.; Becucci, M.; Pavone, M.; Barone, V. On the Properties of Microsolvated Molecules in the Ground (S-0) and Excited (S-1) States: The Anisole-Ammonia 1:1 Complex. *J. Chem. Phys.* **2007**, *127*, 144303, DOI: 10.1063/1.2767265

54 Mazzoni, F.; Becucci, M.; Rezac, J.; Nachtigallova, D.; Michels, F.; Hobza, P.; Muller-Dethlefs, K. Structure and Energetics of the Anisole-Ar-N (N = 1, 2, 3) Complexes: High-Resolution Resonant Two-Photon and Threshold Ionization Experiments, and Quantum Chemical Calculations. *Phys. Chem. Chem. Phys.* **2015**, *17*, 12530– 12537, DOI: 10.1039/C5CP01166C

55 Rezac, J.; Nachtigallova, D.; Mazzoni, F.; Pasquini, M.; Pietraperzia, G.; Becucci, M.; Muller-Dethlefs, K.; Hobza, P. Binding Energies of the Pi-Stacked Anisole Dimer: New Molecular Beam-Laser Spectroscopy Experiments and Ccsd(T) Calculations. *Chem. - Eur. J.* **2015**, *21*, 6740– 6746, DOI: 10.1002/chem.201406134

56 Ringer, A. L.; Figgs, M. S.; Sinnokrot, M. O.; Sherrill, C. D. Aliphatic C-H/Pi Interactions: Methane-Benzene, Methane-Phenol, and Methane-Indole Complexes. *J. Phys. Chem. A* **2006**, *110*, 10822– 10828, DOI: 10.1021/jp062740l

57 Zhang, X.; Knee, J. L. Dynamics of Large Molecule Van-Der-Waals Complexes Studied with Zeke Spectroscopy. *Faraday Discuss.* **1994**, *97*, 299– 313, DOI: 10.1039/fd9949700299

58 Dey, R. C.; Seal, P.; Chakrabarti, S. Ch/Pi Interaction in Benzene and Substituted Derivatives with Halomethane: A Combined Density Functional and Dispersion-Corrected Density Functional Study. *J. Phys. Chem. A* **2009**, *113*, 10113– 10118, DOI: 10.1021/jp905078p

59 Schauer, M.; Law, K. S.; Bernstein, E. R. Molecular Jet Study of the Solvation of Toluene by Methane, Ethane, and Propane. *J. Chem. Phys.* **1985**, *82*, 736– 746, DOI: 10.1063/1.448497

60 CNRS *Lv_Pbasex,* 2.10; Iramis CEA, **2013**.

61 Frisch, M. J.; Trucks, G. W.; Schlegel, H. B.; Scuseria, G. E.; Robb, M. A.; Cheeseman, J. R.; Scalmani, G.; Barone, V.; Petersson, G. A.; Nakatsuji, H.; *Gaussian 09;* Gaussian, Inc: Wallingford, CT, **2009**.

62 Sinnokrot, M. O.; Sherrill, C. D. Highly Accurate Coupled Cluster Potential Energy Curves for the Benzene Dimer: Sandwich, T-Shaped, and Parallel-Displaced Configurations. *J. Phys. Chem. A* **2004**, *108*, 10200– 10207, DOI: 10.1021/jp0469517

63 Perdew, J. P.; Ernzerhof, M.; Burke, K. Rationale for Mixing Exact Exchange with Density Functional Approximations. *J. Chem. Phys.* **1996**, *105*, 9982– 9985, DOI: 10.1063/1.472933

64 Adamo, C.; Barone, V. Accurate Excitation Energies from Time-Dependent Density Functional Theory: Assessing the Pbe0Model for Organic Free Radicals. *Chem. Phys. Lett.* **1999**, *314*, 152– 157, DOI: 10.1016/S0009-2614(99)01113-6

65 Grimme, S.; Antony, J.; Ehrlich, S.; Krieg, H. A Consistent and Accurate Ab Initio Parametrization of Density Functional Dispersion Correction (Dft-D) for the 94 Elements H-Pu. *J. Chem. Phys.* **2010**, *132*, 154104, DOI: 10.1063/1.3382344

66 Weigend, F. Accurate Coulomb-Fitting Basis Sets for H to Rn. *Phys. Chem. Chem. Phys.* **2006**, *8*, 1057– 1065, DOI: 10.1039/b515623h

67 Weigend, F.; Ahlrichs, R. Balanced Basis Sets of Split Valence, Triple Zeta Valence and Quadruple Zeta Valence Quality for H to Rn: Design and Assessment of Accuracy. *Phys. Chem. Chem. Phys.* **2005**, *7*, 3297– 3305, DOI: 10.1039/b508541a

68 Talipov, M. R.; Boddeda, A.; Timerghazin, Q. K.; Rathore, R. Key Role of End-Capping Groups in Optoelectronic Properties of Poly-P-Phenylene Cation Radicals. *J. Phys. Chem. C* **2014**, *118*, 21400– 21408, DOI: 10.1021/jp5082752

69 Renz, M.; Theilacker, K.; Lambert, C.; Kaupp, M. A Reliable Quantum-Chemical Protocol for the Characterization of Organic Mixed-Valence Compounds. *J. Am. Chem. Soc.* **2009**, *131*, 16292– 16302, DOI: 10.1021/ja9070859

70 Renz, M.; Kess, M.; Diedenhofen, M.; Klamt, A.; Kaupp, M. Reliable Quantum Chemical Prediction of the Localized/Delocalized Character of Organic Mixed-Valence Radical Anions. From Continuum Solvent Models to Direct-Cosmo-Rs. *J. Chem. Theory Comput.* **2012**, *8*, 4189– 4203, DOI: 10.1021/ct300545x

71 Hoffmann, L. J. H.; Marquardt, S.; Gemechu, A. S.; Baumgartel, H. The Absorption Spectra of Anisole-H8, Anisole-D3 and Anisole-D8. The Assignment of Fundamental Vibrations in the S-0 and the S-1 States. *Phys. Chem. Chem. Phys.* **2006**, *8*, 2360– 2377, DOI: 10.1039/B600438P

72 Gemechu, A. S.; Hoffmann, L. J. H.; Marquardt, S.; Eisenhardt, C. G.; Baumgartel, H.; Chelli, R.; Cardini, G.; Califano, S. The Absorption Spectrum of Anisole and the Anisole/Co2 1:1-Cluster. The Influence of Intermolecular Interaction on Intramolecular Vibrations. *Z. Phys. Chem.* **2004**, *218*, 123– 153, DOI: 10.1524/zpch.218.1.123.25390

73 Schauer, M.; Bernstein, E. R. Molecular Jet Study of the Solvation of Benzene by Methane, Ethane, and Propane. *J. Chem. Phys.* **1985**, *82*, 726– 735, DOI: 10.1063/1.448496

74 Eisenhardt, C. G.; Gemechu, A. S.; Baumgartel, H.; Chelli, R.; Cardini, G.; Califano, S. Excited State Photoelectron Spectroscopy of Anisole. *Phys. Chem. Chem. Phys.* **2001**, *3*, 5358– 5368, DOI: 10.1039/b105106g

75 Pradhan, M.; Li, C. Y.; Lin, J. L.; Tzeng, W. B. Mass Analyzed Threshold Ionization Spectroscopy of Anisole Cation and the Och3 Substitution Effect. *Chem. Phys. Lett.* **2005**, *407*, 100– 104, DOI: 10.1016/j.cplett.2005.03.068

76 Kokkin, D.; Ivanov, M. V.; Loman, J.; Cai, J.-Z.; Rathore, R.; Reid, S. A. Strength of Π-Stacking, from Neutral to Cation: Precision Measurement of Binding Energies in an Isolated Π-Stacked Dimer. *J. Phys. Chem. Lett.* **2018**, *9*, 2058– 2061, DOI: 10.1021/acs.jpclett.8b00742

77 Ruckenstein, E.; Shulgin, I. L.; Tilson, J. L. The Structure of Dilute Clusters of Methane and Water by Ab Initio Quantum Mechanical Calculations. *J. Phys. Chem. A* **2003**, *107*, 2289– 2295, DOI: 10.1021/jp022267l